Journal of Ceramic Processing Research. Vol. 25, No. pp. 278~284 (2024)
(Received 29 January 2024, Received in revised form 8 March 2024, Accepted 19 March 2024)
https://doi.org/10.36410/jcpr.2024.25.. '8

J O U R N A L O F
Ceramic Processing Research

Examining the temperature at which magnesium titanates undergo phase formation in the presence of various sintering accelerators

Ping-Cheng Chen[a], Chung-Long Pan[b], Kuei-Chih Lin[c] and Chun-Hsu Shen[c,*]
[a]*Department of Intelligent Network Technology, I-Shou University, No.1, Sec. 1, Syuecheng Rd., Dashu District, Kaohsiung City 84001, Taiwan*
[b]*Department of Electrical Engineering, I-Shou University, No.1, Sec. 1, Syuecheng Rd., Dashu District, Kaohsiung City 84001, Taiwan*
[c]*Department of Electronic Engineering, Ming Chuan University, 5 De Ming Rd., Gui Shan District, Taoyuan City 333, Taiwan*

The lower phase-forming temperature of magnesium titanate, $MgTiO_3$, means that it can be used to replace magnesium ions with cobalt ions at 0.05 mole when a mixture of diverse low melting point materials as sintering accelerators is employed (single: B_2O_3, CuO, V_2O_5, ZnO; binary: ZnO-B_2O_3). The phase formation of $0.9Mg_{0.95}Co_{0.05}TiO_3$ - 0.1 $Ca_{0.61}Nd_{0.78/3}TiO_3$ dielectric ceramics was verified using XRD diffraction to observe crystallites at different phases. SEM was used to observe the grain growth of the ceramic system, and the composition ratio of the grain was analyzed via EDS. Compared with $0.9Mg_{0.95}Co_{0.05}TiO_3$ - 0.1 $Ca_{0.61}Nd_{0.78/3}TiO_3$ dielectric ceramics without the addition of a sintering accelerator, the results show that the sintering temperature could be effectively decremented, and the results of the binary addition were better than the single result. The microwave dielectric performances of $0.9Mg_{0.95}Co_{0.05}TiO_3$ - $0.1Ca_{0.61}Nd_{0.78/3}TiO_3$ dielectric ceramics were closely related to the density and growth of grains experienced by the specimens. When 1 wt% binary sintering accelerators (ZnO-B_2O_3) were added to $0.9Mg_{0.95}Co_{0.05}TiO_3$-0.1 $Ca_{0.61}Nd_{0.78/3}TiO_3$ dielectric ceramics, they showed an ε_r value of 21.7, a Qf value of 42,000 GHz, and a τ_f value of -27.2 ppm/°C; the phase-forming temperature was minimized from 1350 °C to 1150 °C.

Keywords: Dielectric ceramics, Phase-forming, Microwave dielectric performances, Sintering accelerator.

Introduction

In recent years, there has been continuous progress made in the semiconductor chip manufacturing process, whether for processing technology or material research and development. Within this, dielectric ceramic materials have also attracted considerable attention due to their lower cost and high microwave characteristics. In early communications, dielectric ceramic materials were mainly used in substrate materials for the production of RF spectrum or microwave system elements (such as tunable filters, amplifiers, oscillators, etc.) [1-4]. Recent applications of microwave components have mainly been applied to dielectric resonators, antennas, filters, etc. [5]. The reason why dielectric ceramics can be used in the field of microwave communication is mainly because of their resistance to the influence of environmental factors (such as humidity, oxidation resistance, appropriate hardness, etc.); they also have a high relative dielectric coefficient (ε_r) and magnetic permeability (u). In addition, the size of the microwave component is proportional to $\sqrt{\lambda_0/\varepsilon_r}$, where λ_0 is the wavelength of the vacant space and ε_r is the relative permittivity of dielectric ceramics; therefore, to reduce the size of the microwave component, a substrate composition with a higher relative permittivity needs to be designated [6-9].

Magnesium titanate has always garnered widespread concern because of its high-quality factor (Qf value) and its dielectric performances, which are ε_r ~ 17, a Qf ~ 160,000 GHz, τ_f ~ -51 ppm/°C [10-12]. In the past, we have attempted to replace magnesium ions with 0.05 mole of cobalt ions in a partial substitution manner, and the formation of $Mg_{0.95}Co_{0.05}TiO_3$ (MCT) has obtained excellent dielectric characteristics with an ε_r of 16.8, a Qf of 230,000 GHz, and a τ_f of -54 ppm/°C [13,14]. However, due to its two disadvantages, including negative temperature characteristics and a high phase-forming temperature, it is limited in practical applications. To overcome the disadvantage of negative temperature characteristics, we attempted to mix it with materials that have extremely high positive temperature coefficients (τ_f) (such as $CaTiO_3$ ~ +800 ppm/°C, $Ca_{0.6}La_{0.8/3}TiO_3$ ~ +213 ppm/°C, $Ca_{0.61}Nd_{0.78/3}TiO_3$ ~ +270 ppm/°C) to compensate for their temperature coefficients, obtaining promising results [13-16].

In this study, we selected a mixture of $Mg_{0.95}Co_{0.05}TiO_3$ and $Ca_{0.61}Nd_{0.78/3}TiO_3$ (CNT) ceramic systems, and when

*Corresponding author:
Tel : +886 3 350-7001 ext. 3737
Fax: +886 3 359-3877
E-mail: chshen0656@mail.mcu.edu.tw

the ratio of $Mg_{0.95}Co_{0.05}TiO_3$ and $Ca_{0.61}Nd_{0.78/3}TiO_3$ was 9:1 (9MCT–CNT), microwave dielectric performances resulted in $\varepsilon_r \sim 22.1$, $Qf \sim 102{,}000$ GHz, $\tau_f \sim -25.4$ ppm/°C. However, this still presented with the disadvantage of a sintering temperature up to 1350 °C, which needed to be overcome. Typically, there are three ways to reduce the phase-forming temperature: the sol-gel process, decreasing the particle size of the initial powder, and adding glass phase composition with a low melting point. Considering the complexity and cost of these processes, we chose to add low melting point materials to the experiments, as many past results have been published in this area [17-25]. We used single and binary additions (single additions: B_2O_3, CuO, V_2O_5, ZnO; binary additions: ZnO-B_2O_3) to observe the change in the phase-forming temperature separately. The microwave dielectric performances were assessed by examining the densification, X-ray diffraction patterns, and microstructures of the ceramics. The microstructures employed SEM (scanning electron microscopy) and EDS (energy-dispersive spectroscopy) to observe changes in the grain, grain boundaries, and compositions of the phases. The association between microstructure and dielectric properties was further investigated, considering variations in the types and concentrations of sintering accelerators.

Experimental Procedure

In this experiment, the required $Mg_{0.95}Co_{0.05}TiO_3$ and $Ca_{0.61}Nd_{0.78/3}TiO_3$ phases were formulated first with a high-purity powder: magnesium oxide (MgO), cobalt oxide (CoO), calcium carbonate ($CaCO_3$), neodymium oxide (Nd_2O_3), and titanium dioxide (TiO_2). To remove the hygroscopicity of magnesium oxide, it had to dry at 600 °C for 2 hours. The required phases were weighed according to the appropriate mole composition ratio, placed into a ball grinding pot, and evenly mixed with agate beads and dis-tilled water before ball grinding was carried out for about 24 h. All mixtures were dried, pounded, sieved, and pre-phased (calcine) at 1100 °C for 4 h ($Mg_{0.95}Co_{0.05}TiO_3$) or 3 h ($Ca_{0.61}Nd_{0.78/3}TiO_3$) in a high-temperature furnace. Then, the pre-phased reagents were formulated again according to the chemical molar ratio of 0.9 $Mg_{0.95}Co_{0.05}TiO_3$ - 0.1 $Ca_{0.61}Nd_{0.78/3}TiO_3$ with various types and contents of sintering accelerators (single: B_2O_3, CuO, V_2O_5, ZnO; binary: ZnO-B_2O_3). They were then re-grounded into a fine powder for 24 h. Afterward, the pre-phased reagents were combined with 3 wt% of a 10% solution of PVA (PVA 500; Showa, Tokyo, Japan) as a binder, and, after complete granulation, uniformity was achieved; they were screened through a sifter (100-mesh) and pressed into an ingot with a thickness of 5 mm and a diameter of 11 mm with a pressure of 200 MPa in a uniaxial hydraulic. The ingot was sintered at 1100 °C-1300 °C for 4 h in the air. Both heating and cooling rates for the apparatus were set at 10 °C per minute to ensure consistent sintering conditions for each sample.

Crystalline phase inspections of both pre-phased powder and mixed compositions were performed using a Siemens D5000 X-ray powder diffractometer (XRD) in Munich, Germany, with Cu-Kα radiation operating at 40 kV and 40 mA. The scanning speed and step size of XRD analysis for the sample were set at 2 degrees/minute and 0.06°. The two-theta range was set between 20 and 60 degrees. XRD data analysis and the calculation of lattice constants were performed using DIFFRAC software. Scanning electron microscopy (SEM; Philips XL-40FEG, Eindhoven, the Netherlands) was utilized to examine the structural features on specimen surfaces, while an energy-dispersive X-ray spectrometer (EDS) was employed to identify and disclose the composition of mixed phases. The Archimedes method was utilized to measure the apparent densities of the mixed compositions. The Hakki-Coleman dielectric resonator method was utilized to measure the relative permittivity (ε_r) and quality factors (Qf) at radio frequencies [26, 27].

The examination system mainly consisted of a vector network analyzer (HP8757D) and HP8350B sweep oscillator connections. The thermal coefficients (τ_f) of these mixed compositions were assessed by keeping the DR inside a temperature-controlled stove with a temperature range of 20 °C to 80 °C. The following formula was utilized to obtain τ_f (ppm/°C): by tracking the shift in the resonance peak frequency of the TE_{011} mode as the temperature slowly changed from 20 °C to 80 °C, τ_f could be calculated from the following equation:

$$\tau_f = \frac{f_2 - f_1}{T_2 - T_1}$$

where f_1 and f_2 represent the resonant frequencies at T_1=20 °C and T_2=80 °C, respectively.

Results and Discussion

The XRD diffraction patterns recorded with 1 wt% binary sintering accelerators (ZnO-B_2O_3) using 9MCT–CNT ceramics at varying sintering temperatures (1100-1200 °C) for 4 hr are presented in Fig. 1. As shown in the figure, this is a two-phase coexisting system, which uses the MCT ceramic (JCPDS #06-0494) as the primary phase alongside the secondary phase, which consists of an ilmenite structure that coexists with the CNT ceramic (JCPDS #22-0153), producing a pseudo-cubic perovskite structure. It can be seen from the figure that, in addition to the coexistence of the above two phases, there is also a very small number of secondary phases ($MgTi_2O_5$: JCPDS #82-1125). The main reasons behind second-phase formation included an increase in the possibility of secondary crystallization nucleation due to the uneven particle size of the initial powder, an increase in the activity rate of grain boundaries due to their high sintering

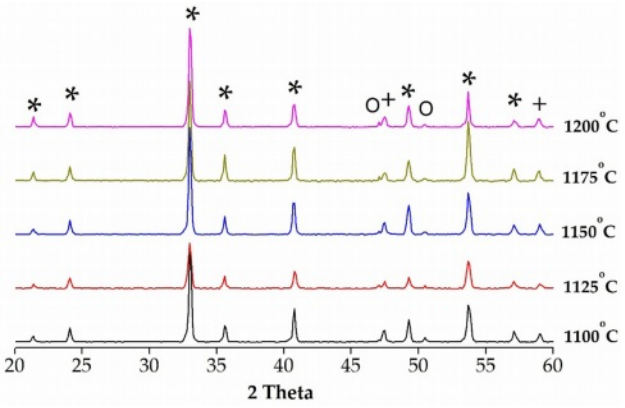

Fig. 1. The XRD results of 9MCT–CNT ceramics after adding 1 wt% ZB at different phase-forming temperatures (*, ilmenite; +, perovskite; ○, $MgTi_2O_5$).

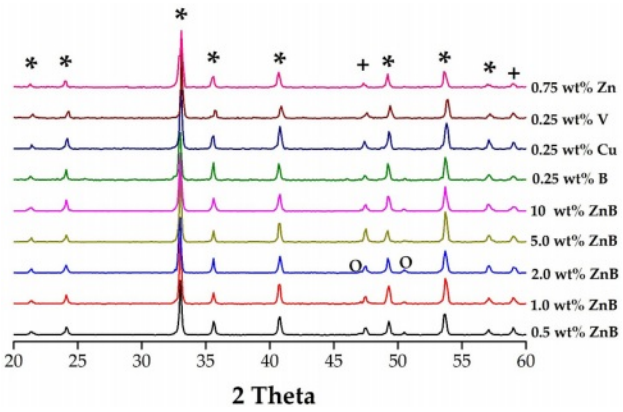

Fig. 2. The XRD results of 9MCT–CNT ceramics with various types and contents of sintering accelerators at their optimum phase-forming temperatures (*, ilmenite; +, perovskite; ○, $MgTi_2O_5$).

temperature, or the local inhomogeneous liquid phase. In addition, the emergence of the second phase ($MgTi_2O_5$) mainly occurs when the proportion of magnesium oxide to titanium dioxide is 1:2; it forms an intervening phase in the micro-structure of the composition that cannot be completely removed [20, 28].

The lattice parameters and phase ratio of 9MCT–CNT ceramics with 1 wt% binary sintering accelerators ($ZnO\text{-}B_2O_3$) sintered at varied temperatures for 4 h are shown in Table 1. It is clear from the table that, due to the rise in sintering temperatures leading to an increase in the grain boundary movement, the ratio of MCT also increased. The reason for this decrease in the ratio of second phases was mainly due to an insufficient sintering temperature. In addition, it could be observed that the lattice parameters of the MCT did not change significantly due to the addition of CNT or a sintering accelerator.

The XRD diffraction patterns recorded with various types and contents of sinter-ing accelerators (single: B_2O_3, CuO, V_2O_5, ZnO; binary: $ZnO\text{-}B_2O_3$) for 9MCT-CNT ceramics are presented in Fig. 2. These varied accelerators did not influence the phase formation of 9MCT-CNT ceramics; however, the second phase ($MgTi_2O_5$) could still be observed. As mentioned earlier, an unintended second phase ($MgTi_2O_5$) generation might affect the dielectric performance of the overall ceramic system [29]. The phase-forming temperature of the $MgTi_2O_5$ phase needed to be as high as 1450 °C; therefore, the higher the phase-forming temperature in the ceramic system, the more severe the influence of the $MgTi_2O_5$ phase [30]. The lattice parameters of 9MCT–CNT ceramics with various types and contents of sintering accelerators at their optimum phase-forming temperatures for 4 h are shown in Table 2. As the content of binary accelerators ($ZnO\text{-}B_2O_3$) increased, the ratio of second phases ($MgTi_2O_5$) decreased, mainly due to the decrease in the phase-forming temperature. All additions could be considered multiphase coexistence systems, with $MgTiO_3$ as the main phase [JCPDS #06-0494, $a = b = 5.054$ (Å), $c = 13.898$ (Å)]. When magnesium (Mg^{2+}) ions were replaced by 0.05 moles of cobalt ions (Co^{2+}), there was a local slight difference in the lattice constant of $MgTiO_3$, mainly because of the difference in ion radius (Co: 0.82 Å, Mg: 0.78 Å). When mixed with CNT, the lattice constant of MCT did not change significantly. The MCT and CNT form a two-phase coexistence system because of structural differences, where Mg^{2+} (0.78 Å) and Co^{2+} (0.82 Å) are smaller than Ca^{2+} (1.06 Å) and Nd^{3+} (1.15 Å) in average ion radii. This verifies the coexistence of a multiphase system for the MCT-CNT ceramic, with MCT as the primary crystalline phase and CNT as the second phase

Table 1. The lattice parameters of 9MCT–CNT ceramics with 1 wt% binary sintering accelera-tors ($ZnO\text{-}B_2O_3$) sintered at varied temperatures for 4 h. Each phase proportion was determined by the peak areas of XRD results.

9MCT-CNT-1wt% ZB					
S.T.(°C)	a(Å)	c(Å)	MCT(%)	CNT(%)	$MgTi_2O_5$(%)
1100	5.0417±0.0104	13.8609±0.0376	90.1	8.02	1.87
1125	5.0480±0.0112	13.8671±0.0409	90	8.01	1.97
1150	5.0417±0.0104	13.8609±0.0376	90.07	7.98	1.94
1175	5.0642±0.0077	13.9236±0.0279	92.55	6.45	0.99
1200	5.0417±0.0104	13.8609±0.0376	89.47	7.78	2.75

Table 2. The lattice parameters of 9MCT–CNT ceramics with various types and contents of sintering accelerators at their optimum phase-forming temperatures for 4 h. Each phase proportion was determined by the peak areas of XRD results.

9MCT–CNT - sintering accelerators					
	a(Å)	c(Å)	MCT(%)	CNT(%)	$MgTi_2O_5$(%)
0.25 wt% B	5.0529±0.0115	13.8804±0.0418	91.96	5.91	2.13
0.25 wt% Cu	5.0591±0.0058	13.8417±0.0209	90.81	8.51	0.68
0.25 wt% V	5.0599±0.0280	13.8560±0.1007	91.54	7.64	0.82
0.75 wt% Zn	5.0411±0.0160	13.8473±0.0579	91.27	7.73	0.99
0.5 wt% ZB	5.0529±0.0115	13.8804±0.0418	89.71	8.04	2.25
1.0 wt% ZB	5.0417±0.0104	13.8609±0.0376	90.07	7.98	1.94
2.0 wt% ZB	5.0417±0.0104	13.8609±0.0376	90.59	7.53	1.88
5.0 wt% ZB	5.0642±0.0077	13.9236±0.0279	89.86	8.67	1.47

in Fig. 1. The above analysis results show that the type and content of the added accelerator do not affect the lattice parameters of the MCT.

Fig. 3 shows the secondary electron SEM micrographs of 9MCT-CNT ceramics with 1wt% binary accelerators (ZnO-B_2O_3) when sintered at varied temperatures. This can be seen in Fig. 3 a to c, where the particle size in the microstructure clearly in-creases with the rise in sintering temperature, and the porosity in Figs. 3a and b is quite high. When the phase-forming temperature increases (1100 °C~1150 °C), the porosity decreases as the grains grow; this is due to the heat driven energy that connects the grains with the expansion of the neck. Therefore, Fig. 3a-c demonstrates grain growth with the more fluid movement of the grain boundary alongside a more uniform and dense structure. However, when the temperature rises above 1150 °C, the grains show excessive growth, mainly due to the excessive extrusion between the grain and air pressure [31-35]. For an extensive investigation into the structure and

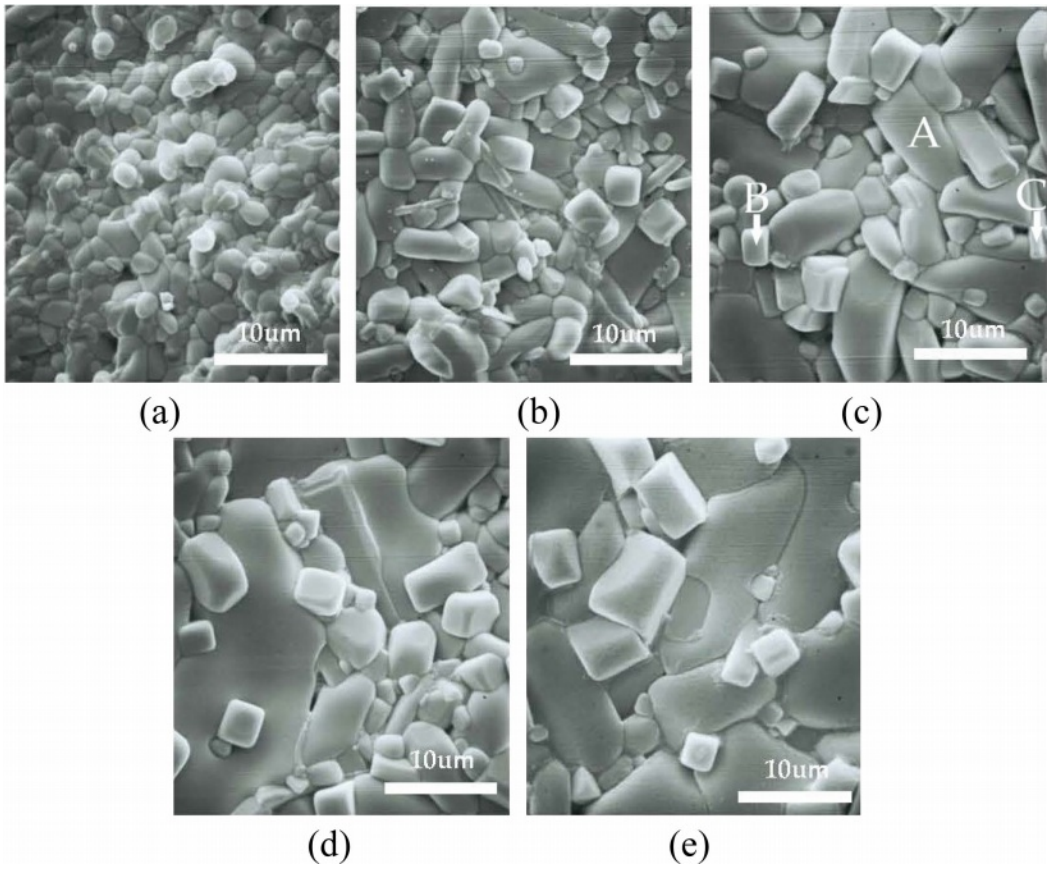

Fig. 3. The SEM images of 9MCT-CNT ceramics were obtained with 1 wt% binary sintering accelerators (ZnO-B_2O_3) at (a) 1100 °C, (b) 1125 °C, (c) 1150 °C, (d) 1175 °C, and (e) 1200 °C for 4 h.

Table 3. The EDS results of particle formation for spots A, B, and C are in Fig. 3(c).

	Atom (%)					
Spot	Mg	Co	Ca	Nd	Ti	O
A	28.16	3.63	0	0	33.66	34.55
B	0	0	25.11	14.5	36.59	23.80
C	16.83	2.81	0	0	43.86	36.51

composition of 9MCT-CNT ceramics with 1 wt% binary accelerators (ZnO-B_2O_3), the EDS results of the SEM image represented in Fig. 3c for spots A-C are shown in Table 3. Therefore, the varied grains are distinguished as follows: spot A is $Mg_{0.95}Co_{0.05}TiO_3$; spot B is $Ca_{0.61}Nd_{0.78/3}TiO_3$, and spot C is the second phase ($MgTi_2O_5$). The results of EDS and XRD analysis were consonant, corroborating that 9MCT-CNT ceramics is a three-phase coexistence system.

The results of the apparent density and dielectric constant (ε_r values) of 9MCT-CNT ceramics, using various types and contents of accelerators sintered at various temperatures, are shown in Fig. 4. At low temperatures (1100 °C), porosity in the structure was high because the driving force of thermal energy was not enough to promote the neck connection and expansion between the grains. When the temperature increased, the thermal driving force increased, making the grain boundary easier to move and smaller grains easier to dissolve; therefore, the growth of the grain was consistent, porosity was reduced, and the density of the overall structure increased. As can be seen from the figure, the addition of a single sintering accelerator (B_2O_3, CuO, V_2O_5, ZnO) resulted in a limited reduction in the sintering temperature to about 100 °C (from 1350 °C to 1250 °C). Conversely, when a binary sintering accelerator (ZnO-B_2O_3) was added, the sintering temperature could be further diminished to 1150 °C (~ 200 °C). In addition, liquid-phase sintering occurred in 9MCT-CNT ceramics when binary sintering accelerators were added; this was more promotive to accomplishing densification through small-grain dissolution, an increase in the wetting boundary movement rate, and grain reorganization. When compared to the SEM in Fig. 4 for 9MCT-CNT ceramics using a binary sintering accelerator (ZnO-B_2O_3) at 1100 °C/4 h, the particles were smaller, pores sizes were larger, and the density was lower. When the sintering temperature rose to 1150 °C/4 h, the particle size was consistent, the pores shrank less, and density was enhanced. Therefore, when various kinds and contents of low melting point materials were added as sintering accelerators, liquid phase sintering could be formed. When the accelerator content was superabundant, the density was slightly reduced. In general, whether it is a single or binary sintering accelerator, at the appropriate content, the phase-forming temperature can be effectively reduced. However, when the sintering accelerator content is superabundant, the grains grow immoderately, and with a larger particle size, reorganization can be subject to greater resistance; this results in a small number of pores in the boundary, causing difficulties in their release, and means that other factors influence variations in the density and radio-frequency of dielectric performances. The ε_r values could vary widely (19-22.4) for the examined temperatures, suggesting that it is very impressionable to the phase-forming temperature. This can be contrasted with SEM, which raises the sintering temperature, resulting in continuous grain growth, a reduction in pore size, and the densification of the 9MCT-CNT ceramics structure. The optimum dielectric performances obtained by the addition of various types of sintering accelerators to 9MCT-CLT ceramics are listed in Table 4. It is known that the optimal phase-forming temperature for a single accelerator is 1250 °C, while the binary accelerator is 1150 °C.

Fig. 5 illustrates the quality factor (Qf value) and temperature coefficients (τ_f values) of 9MCT-CNT

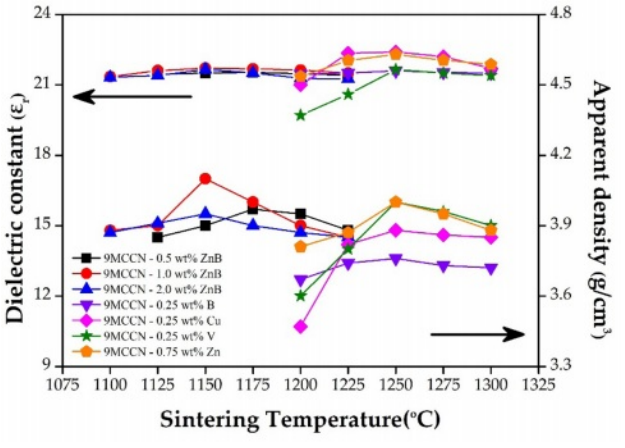

Fig. 4. The apparent density and dielectric constant (ε_r values) of 9MCT-CNT ceramics with various types and contents sintering accelerators at varied temperatures.

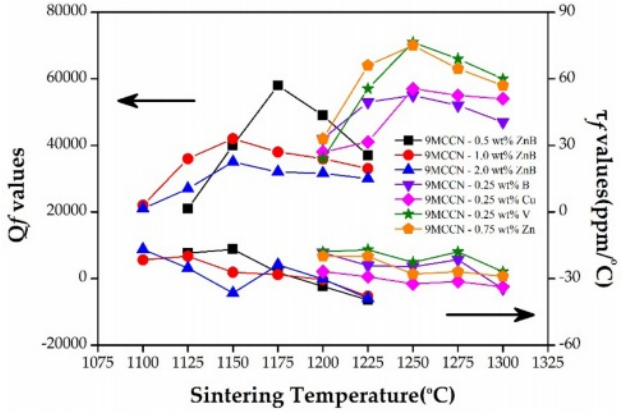

Fig. 5. Qf and τ_f values of 9MCT-CNT ceramics with various types and contents of sintering accelerators at varied temperatures.

Table 4. The dielectric performances with various types of sintering accelerators for 9MCT-CNT ceramics.

Additives	Content(wt%)	S.T.(°C)	D(g/cm^3)	ε_r	*Qf*(GHZ)	τ_f (ppm/°C)
B_2O_3	0.25	1250	3.76	21.6	54,000	-32.4
CuO	0.25		3.88	22.4	57,000	-24.7
V_2O_5	0.25		4.0	21.7	71,000	-22.7
ZnO	0.75		4.0	22.3	70,000	-28
ZnO:B_2O_3	0.5	1175	3.97	21.5	58,000	-27.3
	1.0	1150	4.1	21.7	42,000	-27.2
	2.0	1150	3.95	21.6	35,000	-36.5

ceramics with various types and contents of sintering accelerators at varied temperatures. The *Qf* value is a principal index for dielectric ceramic applications at microwave and millimeter wave frequencies because the *Qf* value is inversely proportional to the dielectric loss experienced by microwave applications. The dielectric loss is the sum of the intrinsic loss and extrinsic loss. The loss in a perfect crystal is the intrinsic dielectric loss, which depends on the interaction between the phonon system and the alternating electric field. The extrinsic dielectric loss is related to defects in the crystal lattice, such as the second phase, oxygen vacancy, inconsistent particle size, and excessive porosity [29, 36-38]. Therefore, density is not only related to the dielectric constant but also impacts the quality factor. Compared with SEM, at low temperatures, the grains are smaller (when the phase is not formed), and the pores are larger; therefore, the density, dielectric constant, and quality factors are lower. When the sintering temperature increases to 1150 °C, the particle size is more accordant (when the phase is formed), the pores are shrunk and reduced, and the overall struc-ture is the most densified due to the sintering of the liquid phase. When 9MCT-CNT ceramics with a 0.5 wt% binary sintering accelerator (ZnO-B_2O_3) are sintered at 1175 °C/4 h, the highest *Qf* value is 58,000 (GHz). When the sintering temperature continues to rise, the quality factor decreases slightly; this can be explained due to immoderate particle growth, an excessive accelerator content, or the second phase of $MgTi_2O_5$. The τ_f of (1–x) $Mg_{0.95}Co_{0.05}TiO_3$ - $xCa_{0.61}Nd_{0.78/3}TiO_3$ is sintered at various temperatures and seems to keep an unchanged value, which is highly correlated with the $Ca_{0.61}Nd_{0.78/3}TiO_3$ contents (x value). The x value of this experiment was 0.1, and the τ_f value did not explicitly vary with the addition of sintering accelerators; it remained unchanged at values of around -22 ~ -36 ppm/°C. This was anticipated because there was no additional phase found throughout the experiment. In addition, the appearance of the second phase ($MgTi_2O_5$) in $Mg_{0.95}Co_{0.05}TiO_3$ ceramics did not lead to a variation in the τ_f value because they possessed congruous ones.

Table 4 shows the results of dielectric performances after adding various types of sintering accelerators to 9MCT-CLT ceramics. It can be seen from the table that whether single or binary additions were used, this could effectively reduce the sintering temperature. The addition of a single sintering accelerator, although reducing the phase-forming temperature, could obtain a higher *Qf* value. The optimal *Qf* value could be obtained using 9MCT-CNT ceramics with 0.25 wt% V_2O_5 at 1250 °C/4 h and 71,000 (GHz). Compared with a single sintering accelerator, the addition of a binary sintering accelerator could reduce the phase-forming temperature by more than 200 °C; however, the *Qf* value of 9MCT-CNT ceramics was greatly reduced due to the excessive sintering of the liquid phase. The optimal *Qf* value was obtained using 9MCT-CNT ceramics with a 1.0 wt% binary sintering accelerator (ZnO-B_2O_3) at 1150 °C/4 h and 42,000 (GHz). Despite the lower dielectric performance of the composition, it was still sufficient to improve the miniaturization of microwave components and the transmission of microwave signals.

Conclusion

The addition of various types (single: B_2O_3, CuO, V_2O_5, ZnO; binary: ZnO-B_2O_3) and contents of sintering accelerators can effectively reduce the phase-forming temperature of 9MCT-CNT ceramics. Compared to 9MCT-CNT ceramics without a sintering accelerator, the phase-forming temperature of 9MCT-CNT ceramics can be reduced from 100 °C (single) to 200 °C (binary) after the addition of a sintering accelerator. Compared to 9MCT-CNT ceramics with a single sintering accelerator (B_2O_3, CuO, V_2O_5, ZnO), 9MCT-CNT ceramics with a binary sintering accelerator (ZnO-B_2O_3) obtained a similar microwave dielectric performance at a lower temperature. When a binary sintering accelerator was added, the generation of second phases ($MgTi_2O_5$) could negatively affect the microwave dielectric properties. The 9MCT-CNT ceramic with a 1.0 wt% binary sintering accelerator (ZnO-B_2O_3) that was sintered at 1150 °C produced the following microwave dielectric performance: a dielectric constant ε_r of 21.7, a *Qf* of 42,000 (GHz), and a τ_f value of -27.2 ppm/°C. The results of these experiments show that, compared with using the pure MCT phase, using the tested composition not only compensates for negative temperature characteristics but

also reduces the phase-forming temperature. Therefore, this composition can be applied to the miniaturization of microwave components, and at the same time, due to a reduction in the sintering temperature, the goal of saving energy and carbon reduction can be achieved.

Acknowledgement

This research was supported by the I-Shou University under grant ISU-112-IUC-02.

References

1. S. Kim, J. Ceram. Process. Res. 18[6] (2017) 421-424.
2. Y.S. Park, E.S. Kim, J. Ceram. Process. Res. 23[6] (2022) 920-926.
3. Y. Jang, J. Kim, S. Kim, K. Lee, IEEE Microw. Wirel. Common. Lett. 24 (2014) 665-667.
4. M.C. Paul, A. Dhar, S. Das, M. Pal, S.K. Bhadra, A. M. Markom, N.S. Rosli, A. Hamzah, H. Ahmad, S.W. Harun, IEEE Photonics J. 7[5] (2015).
5. I.S. Ghosh, A. Hilgers, T. Schlenker, R. Porath, J. Eur. Ceram. Soc. 21 (2001) 2621-2628.
6. P. Palmero, Nanomaterials 5[2] (2015) 656-696.
7. S.J. Penn, N.M. Alford, A. Templeton, X. Wang, M. Xu, M. Reece, K. Schrapel, J. Am. Ceram. Soc. 80 (1997) 1885-1888.
8. L.C. Kretly, A.F.L. Almeida, P.B.A. Fechine, R. S. de Oliveira, A. S. B. Sombra, J. Mater. Sci. Mater. Electron. 15 (2004) 657-663.
9. B. Tang, Q. Xiang, Z. Fang, X. Zhang, Z. Xiong, H. Li, C. Yuan, S. Zhang, Ceram. Int. 45 (2019) 11484-11490.
10. J.H. Sohn, Y. Inaguma, S.O. Yoon, M. Itoh, T. Nakamura, S.J. Yoon, H.J. Kim, Jpn. J. Appl. Phys. 33 (1994) 5466-5470.
11. K. Wakino, Ferroelectrics 91 (1989) 69-86.
12. S. Yuan, L. Gan, F. Ning, S. An, J. Jiang, T. Zhang, Ceram. Int. 44 (2018) 20566-20569.
13. C.L. Huang, C.L. Pan, J.F. Hsu, Mater. Res. Bull. 37 (2002) 2483-2490.
14. C.L. Huang, C.H. Shen, T.C. Lin, J. Alloys Compd. 468 (2009) 516-521.
15. C.H. Shen, S.H. Lin, C.L. Pan, Mater. Res. Bull. 65 (2015) 169-174.
16. A. Ullah, Y. Iqbal, T. Mahmood, A. Mahmood, A. Naeem, M. Hamayun, Ceram. Int. 41 (2015) 15089-15096.
17. C.L. Huang, C.L. Pan, C.C. Yu, J.S. Shen, J. Mater. Sci. 21 (2002) 149-151.
18. C.H. Shen, C.L. Huang, L.M. Lin, C.L. Pan, J. Alloys Compd. 489 (2010) 170-174.
19. C.H. Shen, C.L. Huang, L.M. Lin, C.L. Pan, J. Alloys Compd. 504 (2010) 228-232.
20. C.L. Huang, C.L. Pan, Japan. J. Appl. Phys. 41 (2002) 707-711.
21. H. Yu, T. Luo, J. Liu, J. Adv. Appl. Ceram. 118 (2019) 98-105.
22. C.L. Pan, C.H. Shen, K.C. Lin, Crystals 13[6] (2023) 927.
23. X. Kuang, G. Carotenuto, L. Nicolais, Adv. Perform. Mater. 4 (1997) 257-274.
24. Y.J. Choi, J.H. Park, J. H. Park, S. Nahm, J.G. Park, J. Eur. Ceram. 27[4] (2007) 2017-2024.
25. H.I. Hsiang, C.S. Hsi, C.C. Huang, S.L. Fu, J. Alloy. Compd. 459 (2008) 307-310.
26. B.W. Hakki, P.D. Coleman, IRE Trans. Microwave Theory Tech. 8 (1960) 402-410.
27. W.E. Courtney, IEEE Trans. Microwave Theory Tech. 18 (1970) 476-485.
28. J. Liao, M. Senna, Mater. Res. Bull. 30 (1995) 385-392.
29. B.D. Silverman, Phys. Rev. 125 (1962) 1921-1928.
30. C.L. Huang, C.H. Shen, J. Am. Ceram. Soc. 92 (2009) 384-388.
31. C.L. Huang, S.S. Liu, J. Alloy. Compd. 471 (2009) L9-L12.
32. C.L. Huang, J.J. Wang, Y.P. Chang, J. Am. Ceram. Soc. 90 (2007) 858-862.
33. C.L. Huang, S.S. Liu, S.H. Chen, Jpn. J. Appl. Phys. 48 (2009) 071402-071404.
34. C.L. Huang, J.Y. Chen, J. Alloy. Compd. 485 (2009) 706-710.
35. C.H. Shen, C.L. Pan, Int. J. Appl. Ceram. Technol. 12 (2015) E127-E133.
36. G.L. Gurevich, A.K. Tagantsev, Sov. Phys. JETP. 64 (1986) 142-151.
37. G.L. Gurevich, A.K. Tagantsev, Adv. Phys. 40 (1991) 719-767.
38. D. Kajfezz, P. Guillon, “Dielectric Resonators”, (Noble Publishing Corporation, Atlanta, US 1998).